reviewed paper

Identifying Vulnerable Population under Heat Stress: A Data-Driven Urban Risk Assessment Using Remote Sensing, Citizen Science and Census Data

Marlene Kühnl, Tobias Leichtle, Saskia Rupp, Michael Hiete, Christoph Beck, Christian Geiß, Hannes Taubenböck

(M.Sc. Marlene Kühnl, Company for Remote Sensing and Environmental Research (SLU), Kohlsteiner Str. 5, 81243 München, Germany, marlene.kuehnl@slu-web.de)
(Dr. Tobias Leichtle, German Aerospace Center (DLR), German Remote Sensing Data Center (DFD), Münchner Str. 20, 82234, Wessling, Germany, tobias.leichtle@dlr.de)
(M. Sc. Saskia Rupp, Institute for Theoretical Chemistry, Universität Ulm, Helmholtzstr. 18, 89081, Ulm, Germany, saskia.rupp@uni-ulm.de)
(Prof. Dr. Michael Hiete, Institute for Theoretical Chemistry, Universität Ulm, Helmholtzstr. 18, 89081, Ulm, Germany, michael.hiete@uni-ulm.de)
(Prof. Dr. Christoph Beck, Institute for Geography, Universität Augsburg, Alter Postweg 118, 86159, Augsburg, Germany, Christoph.beck@geo.uni-augsburg.de)
(Prof. Dr. Christian Geiß, German Aerospace Center (DLR), Münchener Straße 20, 82234 Wessling; Geographisches Institut der Universität Bonn, Universität Bonn, 53115 Bonn, christian.geiss@dlr.de)
(Prof. Dr. Hannes Taubenböck, German Aerospace Center (DLR), Münchener Straße 20, 82234 Wessling; Institute for Geography and Geology, Julius-Maximilians-Universität Würzburg, 97074 Würzburg, hannes.taubenboeck@dlr.de)

DOI: 10.48494/REALCORP2026.0144

1 ABSTRACT

Cities are increasingly confronted with rising temperatures and more frequent heatwaves, posing significant challenges for urban resilience and spatial planning. In this study, we investigate heat exposure and its interaction with social vulnerability in the cities of Augsburg, Zwickau and Hamm, Germany, based on remotely sensed, geo- andcensus data as well as citizen science air temperature data. A comprehensive 2.5D urban model was developed, integrating 30 different parameters such as vegetation shares, impervious surfaces, and building parameters like density or floor area ratio, as well as spectral characteristics like Normalised Difference Vegetation Index (NDVI) or satellite-based Land Surface Temperature (LST). In combination with citizen science (‘gathered by the public’) air temperature data measurements, it enabled 100m resolution modelling of heatwave peaks. Machine-learning techniques (Random Forest, RF) and multivariate techniques, particularly Partial Least Squares (PLS) regression, performed convincingly in handling the uncertainties inherent in citizen-science air temperature loggers and ensured robust, area-wide heat wave exposure predictions.

In parallel to modelling heatwave exposure, social vulnerability was assessed using the 2022 census data in Germany. Age structure serves as the core vulnerability indicator, with residents above 65 identified as particularly sensitive, and younger cohorts considered moderately vulnerable compared to the remainder of the population. Merging the information on social vulnerability with the modelled heat exposure, an exposure weigheted Heat Vulnerability Index (HVI) was created at the grid level, revealing spatial patterns of heat risk across the three cities.TheHVI highlights the most heat-endangered urban areas where residents are most likely to suffer from heat.

The findings provide a robust evidence base for municipal adaptation strategies and risk-sensitive planning. The study underscores that meaningful heat-risk assessment is only possible throughintegration of social vulnerability, and that its spatial granularity is crucial for designing effective, locally adapted measures to enhance urban resilience.

Keywords: Heatrisk, Social Vulnerability, Heat Exposure, Population, Heat Vulnerability Index

2 INTRODUCTION

Worldwide, many cities experience extreme heat and rising exposures are projected for the future (Friesen & Taubenböck, 2025, IPCC, 2022). It has become one of the most critical climate-related hazards in urban areas, with increasing morbidity and mortality. The combined influence of global climate change and therefore an increase in the number and severity of heatwaves on the one hand and urban heat island (UHI) effects on the other hand disproportionately affect temperature conditions in cities (Ramachandra et al., 2025, Dodman et al., 2022, Gilabert et al., 2021). The UHI is the product of dense built-up structures, impervious surfaces, limited vegetation,anthropogenic emissions from air conditioning, industries and vehicles, as well as limited airflow. In this process, urban areas experience significantly higher temperatures

than their rural surroundings (Ramachandra et al., 2025, Liu et al., 2024). At the same time, ongoing climate change is leading to an increase inboththe frequency and intensity of heatwaves. In combination with rapid urbanization (Taubenböck et al., 2024) this leads to thermal stress in urban agglomerations and and inceased risk for human health, infrastructure, and urban livability (Dodman et al., 2022, Gilabert et al., 2021).

Remote sensing has become a cornerstone of urban heat analysis and modelling. Its ability to provide information for spatially continuous and temporally consistent observations of land surface temperature (LST) as well as related surface characteristics over large areas stands out (Li et al., 2013, Weng, 2009, Voogt & Oke, 2003). Multiple sensors like Landsat, MODIS, or Sentinel are widely used to identify urban heat hotspots, to quantify the surface UHI (SUHI), and examine the influence of land cover on surface temperatures (e.g. Zargari et al., 2024, Aslan & Koc-San, 2016). However, satellite-derived LST only approximates near-surface air temperature. In complex urban environments, such as street canyons and residential neighbourhoods, LST often fails to capture spatial variability in air temperatures (Li et al., 2013, Voogt & Oke, 2003). Moreover, the heat that people actually experience is defined by air temperature, together with humidity, radiation, and wind (Oke et al., 2017).

To overcome limitations, citizen science (CS) air temperature measurements are increasingly used as input data for urban heat modelling (e.g. Leichtle et al., 2023 a & b). The data are collected via personal, CS weather stations, and stored in publicly accessible servers, providing alternative and low-cost input air temperature data(Meier et al., 2017).Combined with remote sensing data, CS observations improve the spatial resolution of temperature estimates compared to LST data and enable more realistic representations of thermal conditions experienced by urban populations (Fenner et al., 2021, Zumwald et al., 2021).

However, heat-related impacts are not determined by temperature alone. Risk emerges from the combination of thermal exposure and social vulnerability of exposed inhabitants. The latter varies across urban neighbourhoods due to differences in age structure, health status, socioeconomic conditions, housing quality, or access to cooling resources (Weigand et al., 2023, Dodman et al., 2022, Dong et al., 2020).Elderly individuals, young children, people with chronic illnesses, and socioeconomically disadvantaged groups are particularly susceptible to heat stress, often experiencing disproportionate health burdens during extreme heat events (Dodman et al., 2022, Harlan et al., 2013). Integrating vulnerability indicators with remote sensing-based heat metrics is therefore essential to move from heat exposure mapping towards a risk-oriented perspective that better reflects real-world impacts (Dodman et al., 2022; Chen et al., 2018).

Therefore, this study aims to identify urban heat hotspots by jointly considering heat exposure during heatwave conditions and spatially explicit age-related vulnerability. By combining heatwave models based on remotely-sensed landcover and spectral information like Land Surface Temperature, as well as CS air temperature, with socio-demographic vulnerability factors, this paper establishes a Heat Vulnerability Index (HVI) locating the areas within cities posing the greatest risk to human populations. Such an integrated approach aims at a more comprehensive understanding of urban heat risk and aims to support targeted adaptation strategies, informing urban planning, public health interventions, and climate adaptation efforts in cities.

3 MATERIAL AND METHODS

This section introduces the study area, describes the datasets used and their pre-processing steps, and outlines the methodology applied for the heatwave models as well as the HVI.

3.1 Study area

The study was conducted in three mid-sized German cities: Augsburg, Hamm, and Zwickau, each representing distinct urban contexts in terms of geography, demographic structure, and local climate. Their location within Germany is shown in Fig.2, top left.

Augsburg, located in the state of Bavaria in southern Germany, has a population of approximately 308,000 inhabtitants within an area of about 147km² (Stadt Augsburg a, 2026, Amt für Statistik und Stadtforschung der Stadt Augsburg, 2026). The city experiences a warm temperate climate with relatively high precipitation throughout the year (Köppen-Geiger classification Cfb). The summers are warm and the winters cool (Climate-Data.org a, 2026, Beck et al., 2018).

Hamm is situated in the federal state of North Rhine-Westphalia in western Germany and has an estimated population of around 180,500 inhabitants across approximately 226km² (Stadt Hamm a, 2026, Statistisches Bundesamtd, 2026). The city's climate is also classified as warm temperate with mean annual temperatures of 10,3°C and relatively even precipitation throughout the year, accompanied by warm summers and cool winters often near or slightly below freezing (Köppen-Geiger classification Cfb; Climate-Data.org b, 2026, Beck et al., 2018).

Zwickau, located in the state of Saxony in eastern Germany, is the fourth largest city in Saxony with about 87,000 inhabitants and covers roughly 102km² (Stadt Zwickau a & b, 2026). The local climate is similarly temperate with warm summers and cold winters typical of Central Europe, reflecting the Cfb climate regime by Köppen-Geiger with average temperatures of 9,1°C and high precipitation numbers throughout the year (Climate-Data.org c, 2026, Beck et al., 2018). Zwickau's location in the Mulde river valley and its surrounding topography influence local microclimatic conditions. The position in the valley causes a traffic jam of warm air within the heavily overheated districts, especially during summery, windless weather conditions (Stadt Zwickau c, 2026).

Collectively, these three cities represent a range of urban settings in Germany with temperate climates, all of which are increasingly affected by heat stress during summer as a consequence of climate change and the rising frequencyand intensity of heatwaves (Stadt Augsburg b, 2026, Stadt Zwickau c, 2026, Stadt Hamm b, 2026).

3.2 Data

This section presents the datasets used for heatwave modelling (see Section 3.3.1 for a detailed methodological description) and for the identification of age-related population vulnerability. Both datasets serve as input variables for the construction of the HVI, which is described in detail in Section 3.3.2 and is used to spatially assess heat risk across the three test cities.

3.2.1 Input Data for HeatwaveModelling

Citizen Science air temperature data

CStemperature data form one part of the heatwave modelling input for the three test cities. Observations were sourced from two CS sensor networks: Netatmo Citizen Weather Stations and Sensor.Community (formerly Luftdaten.info). Previous studies show that crowdsourced air temperature data are statistically comparable to official meteorological observations, supporting their use in urban climate and heatwave analyses (Leichtle et al., 2023b).

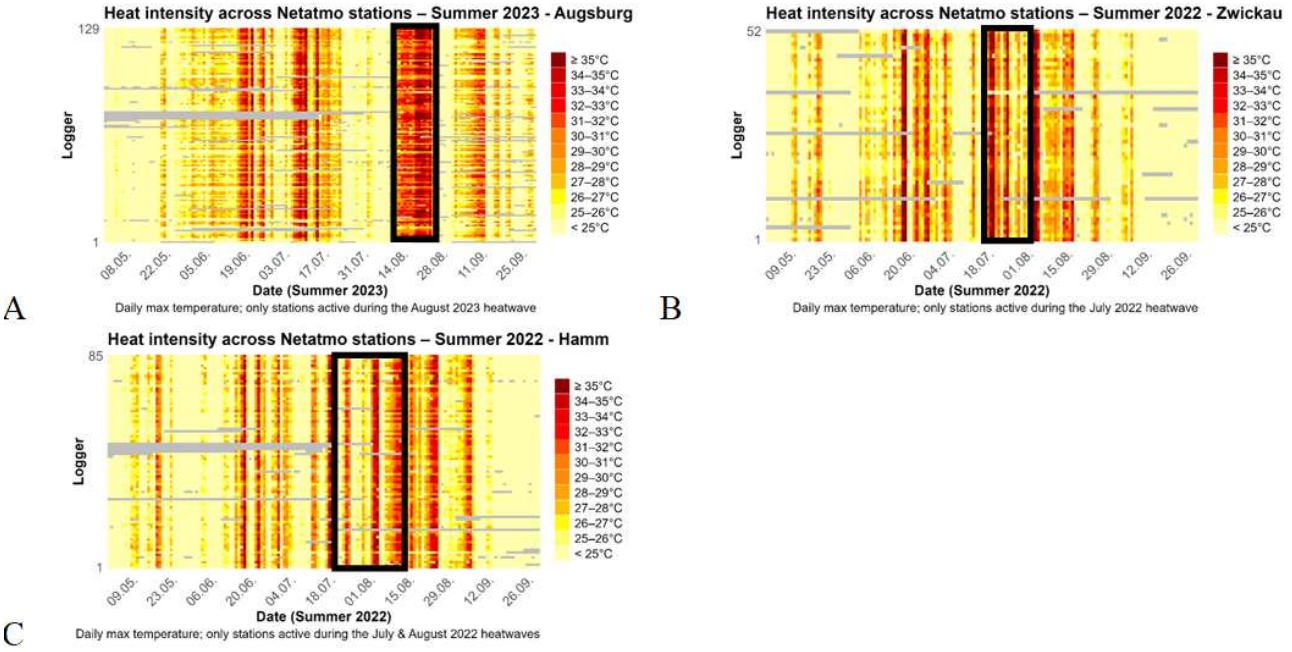

Figure 1: Heat intensity across Netamto stations during summer 2023 for Augsburg (A) and summer 2022 for Zwickau (B), and Hamm (C). In each case, the black box highlights the time period from which the data used in this study were derived.

Editors: M. Schrenk, C. Beyer, T. Popovich, J. Ryser, D. Mawlood
ISBN 978-3-9504945-5-6

Netatmo Citizen Weather Stations are commercial devices produced by the French company Netatmo. The outdoor module measures air temperature and relative humidity at a temporal resolution of five minutes. Data are transmitted automatically and wirelessly to Netatmo serversand, if users consent, are made publicly available and can be collected from the Netatmo network (https://weathermap.netatmo.com/) via the Netatmo Application Programming Interface (API, https://dev.netatmo.com/). For this study, Netatmo data were retrieved for the period August 2023 for Augsburg (13.08.-26.08.2023, 129 loggers, Fig.1A), July 2022 for Zwickau (18.07.-31.07.2022, 52 loggers, Fig.1B) and July and August of 2022 for Hamm (18.07.-12.08.2022, 85 loggers, Fig.1C), representing real time heatwaves visible in the data (Fenner et al., 2021).

The second data source, Sensor.Community, provides environmental data from an open-source sensor network. Data were accessed via the Open Sensor Web platform (now operating under the name Sensoto), which aggregates measurements from multiple open environmental sensor networks (PIKOBYTES GmbH, 2026). Sensor.Community data were also downloaded via an API for the same periods as Netatmo (Hamm: twologgers; Augsburg: eightloggers; Zwickau: twologgers). The sensors are assembled by users themselves and were originally designed for fine dust measurements rather than meteorological observations. The recording resolution is two and a half minutes. The spatial distribution of the loggers from both CS networks is shown in Fig.2.

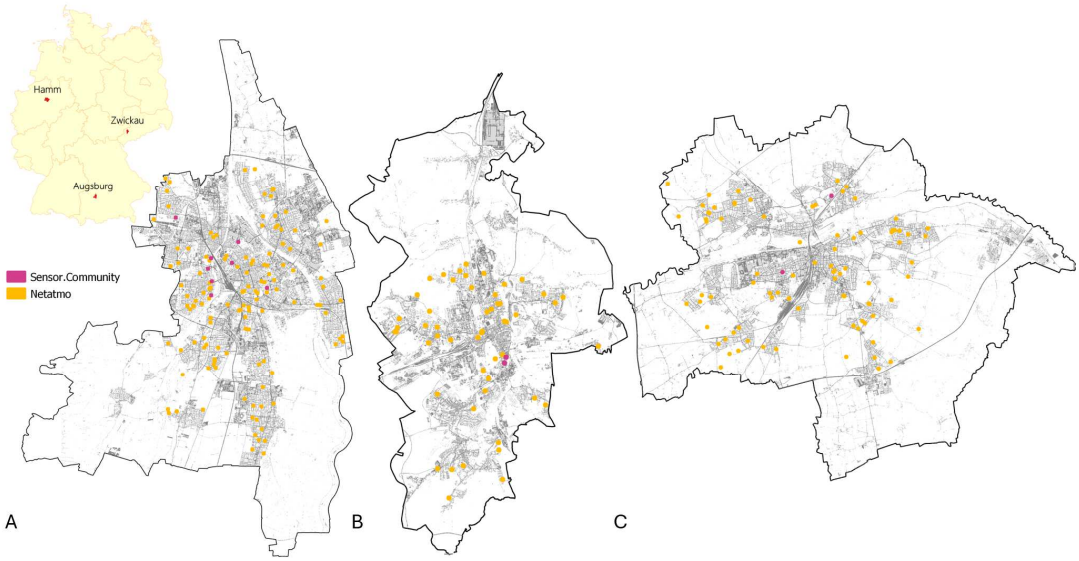

Figure 2: Spatial distribution of the Netatmo (orange) and Sensor.Community (pink) loggers throughout the test cities Augsburg (A), Zwickau (B), and Hamm (C). In Augsburg 129 Netatmo and eight Sensor.Community loggers, in Zwickau 52 Netatmo and two Sensor.Community loggers, and in Hamm 85 Netatmo and two Sensor.Community loggers were applied. In the background, impervious surfaces can be seen.

In contrast to official meteorological stations, data from both CS networks are not subject to formal verification procedures and may exhibit various sources of error. These include issues related to sensor installation, station design (e.g. insufficient ventilation), sensor calibration, and data transmission problems (Fenner et al., 2021). To address these uncertainties, in a first quality-control step, the CS temperature data were adjusted using the CrowdQC+ R package (Fenner et al., 2023), which applies statistical methods to detect and correct measurement biases (Bechtel et al., 2024).

To prepare the data for modelling, daily maximum air temperature values were derived for each CS logger and used as model input. After aggregation, all stations were manually re-evaluated regarding the plausibility of their maximum temperatures. This screening showed that some loggers recorded unusually high temperatures in predominantly vegetated areas, while others showed unexpectedly low values in densely built-up structures, contradicting expected land - temperature relationships (Leichtle et al., 2023a). These inconsistencies were particularly evident in Hamm and Zwickau, where the number of sensors was limited and not all Local Climate Zones (LCZs; Stewart and Oke, 2012) were sufficiently represented (e.g. only one sensor representing industrial areas). As these anomalies were likely related to station design (e.g., insufficient radiation shielding) and only became apparent in relation to surrounding land cover, they were not detected by the standard CrowdQC+ quality control.

As a consequence, for Zwickau and Hamm, a limited number of daily maximum air temperature values were slightly manually adjusted to improve the physical plausibility and representativeness of the temperature input data used for model development.In Hamm, four stations were adjusted: three near vegetated areas were slightly lowered to align with comparable sensors within the test city, while one inner-city station was slightly increased.In Zwickau, one station was slightly lowered, as it recorded one of the highest temperatures citywide despite being located in a green area next to a large water body, where lower readings would typically be expected.

Landcover data

In addition to meteorological data, landuse landcover (LULC) information was used to model heat exposure during heatwave events. For this purpose, LULC classifications derived from very high-resolution (VHR) satellite imagery were employed. The datasets include WorldView-3 imagery for Augsburg acquired on 19th of July 2018 (30 cm spatial resolution), WorldView-2 imagery for Zwickau acquired on 25th of July 2022 (50 cm), and GeoEye imagery for Hamm acquired in 2020, consisting of two images from 27th of April and 8th of May 2020 (40 cm). All three images were obtained from European Space Imaging, EUSI (https://www.euspaceimaging.com/).

Image classification was conducted using the software eCognition. For the VHR WorldView datasets, knowledge-based approaches relying on spectral image characteristics were applied, while the GeoEye dataset was classified using a Convolutional Neural Network (CNN; Montensinos López et al., 2022, Geiß et al., 2022)followed by a knowledge-based post-classification refinement. The final LULC products provide detailed information on vegetation (including height attributes), water bodies, and impervious surfaces, including buildings. Overall accuracies rank from 87% in Zwickau to 94% in Hamm.

The classified land cover data were aggregated to a regular 100 m × 100 m INSPIRE-compliant grid (European Comission, 2013) covering the entire extent of each test city for model application. In addition, a separate 100 m × 100 m grid was generated for the surroundings of the temperature sensor locations to establish relationships between air temperature and land cover characteristics.

Based on the LULC classifications and supplementary geospatial datasets, including normalised digital surface models (nDSMs) and Open Street Map data, a range of additional parameters were derived at the grid-cell level. These include shadow cast at noon and dawn, green volume, climate effective vegetation (cooling effect extending beyond the local site, green spaces ≥ 0.5 hectar, Aram et al., 2019), sky view factor, distance to the city centre, and building-related metrics such as building density, building volume, and floor area ratio.

Furthermore, spectral information from the VHR imagery and additional Landsat-8 data (30 m spatial resolution, retrieved through the Google Earth Engine) were integrated into the grid framework. For each city, Landsat-8 acquisition periods were selected to closely match the acquisition dates of the respective VHR images. Accordingly, Landsat-8 data from April to August 2022 were used for Zwickau, from April to August 2020 for Hamm, and from April to August 2018 for Augsburg. The spectral variables include the Normalized Difference Vegetation Index (NDVI) and surface albedo. Furthermore, Land Surface Temperature (LST) was incorporated as a climatological metric, computed as the mean summer LST over the period 2013-2024 based on all available Landsat-8 data for the summer periods for each respective city.

The final output consists of a spatially comprehensive 100 m × 100 m grid for each test city and an additional grid centered at the locations of the CS temperature measurements, also with a 100m x 100m resolution. Each grid cell contains the full set of derived land cover, structural, and spectral parameters used for heat exposure modeling. An overview over included parameters is shown in Table 1.

Building parameters	Landcover parameters	Describing parameters	Spectral parameters
• Volume • Density • Floor area ratio	• Imperviousness • Water • Vegetation *(all, green volume, climate effective, ≤2m, 2m - ≤10m, 10m - ≤20m, > 20m)*	• Distance to centre • Shadow • Sky View Factor	• NDVI • Albedo • LST

Table 1: Overview of the parameters included in the areawide grid cells covering the test cities and in the grid cells surrounding the logger locations.

Editors: M. Schrenk, C. Beyer, T. Popovich, J. Ryser, D. Mawlood
ISBN 978-3-9504945-5-6

3.2.2 Social Vulnerability

Data from the German Census 2022, provided on a nationwide 100 m × 100 m grid and accessible via the Zensus database (Statistisches Bundesamt a & b, 2022), served as the primary source. Two census datasets were employed:population counts disaggregated into 10-year age groups (<10 years to >80 years; Alter in 10er-Jahresgruppen in Gitterzellen (A), Statistisches Bundesamt a, 2022), andpopulation counts disaggregated into five age classes (<18 years, 18–29 years, 30–49 years, 50–64 years, and ≥65 years; Alter in 5 Altersklassen in Gitterzellen (B), Statistisches Bundesamt b, 2022).Each grid cell stores the number of residents belonging to the respective age group. Grid cells corresponding to the study areas were extracted from these nationwide datasets. As land cover information is available on an INSPIRE-compliant 100 m grid (see Section 3.2.1), the census grids align precisely with the land cover grids within the test cities.

Previous studies have shown that residents aged 65 years and older areparticularly vulnerable to heat stress, while young children and infants also face elevated heat-related risks (e.g. Azan et al., 2015, Arsad et al., 2022, United Nations Children's Fund, 2023, Hajat et al., 2007). Accordingly, these age groups constituted the primary focus of the present analysis. To do so, three data preprocessing steps were carried out. Initially, datasets (A) & (B) were combined into one grid layer. The new grid contains all columns from both data sets. Secondly, to enable a fine-scale assessment of age-specific heat exposure below four years of age, the population below 10 years of age was even further refined using the GENESIS database (Bevölkerung: Kreise, Stichtag, Geschlecht, Altersgruppen, Statistisches Bundesamt c, 2026), which provides city-level relative age-group shares. For the cities of Hamm and Augsburg, the relative shares of children aged <3 years, 3–5 years, and 6–10 years are available. Proportions of these sub-age groups within the total population under 10 years of age were calculated and applied to the 100m census grid cells, resulting in a refined spatial representation of children's age groups. For Zwickau, no city-specific sub-age-group information for children under 10 years was available. In this case, the mean proportions derived from Hamm and Augsburg were used to disaggregate the population under 10 years of age into the same three sub-age groups, ensuring methodological consistency across all study areas. In a third preprocessing step, both census information age intervals were combined. Up until age group 50-59 years, the present paper uses the information from dataset (A), including the newly defined sub-age groups below 10 years of age. Above 60 years of age, based on previous publications, the threshold 65 years and older should be used (e.g. Kohon et al., 2024, Reid et al., 2012). Therefore, this age group from dataset (B) had to be combined with the age classes 60-69 years, 70-79 years and above 80 years from datset (A)to derive the age group 60-64 yearsin order to generate consistent age coverage while using the age group 65 years + from dataset (B) for the analysis. This was achieved by summing the age classes 60–69, 70–79, and ≥ 80 years from (A) and subtracting the 65+ population from (B). As both datasets are stored within the same grid structure, this operation was performed directly at the grid-cell level.

The final age categories used in the analysis are: < 3 years, 3–5 years, 6–9 years, 10-19 years, 20-29 years, 30-39 years, 40-49 years, 50-59 years, 60–64 years, and ≥ 65 years.

3.3 Methodology

3.3.1 Heatwave Modelling with Partial Least Squares Regression or Random Forest and Validation

Partial Least Squares Regression (PLS) and Random Forest (RF) were applied to model maximum air temperature patterns under heatwave conditions in the three test cities Augsburg, Zwickau, and Hamm, using in-situ observations from the CS networks Netatmo and Sensor.Community. PLS was selected as the primary approach because it performs well with limited observations and strong multicollinearity among predictors (Pirouz, 2006), both of which characterise the dataset (e.g., correlations between impervious surfaces, bare soil, and vegetation-related variables). Given the restricted number of CS temperature measurements, this robustness was particularly relevant. For comparison, RF was additionally implemented. As a non-parametric, non-linear method (Breiman, 2001), RF can capture complex relationships between land cover patterns and air temperature and is generally robust to multicollinearity, often outperforming conventional regression approaches, although predictions remain limited to the value range represented in the training data (He et al., 2025; Oukawa et al., 2022; Breiman, 2001).

The model input consisted of daily maximum CS temperature measurements per logger and a set of land cover and spectral variables extracted from grid cells surrounding the sensor locations. Based on these data,

both models established statistical relationships between air temperature and land cover as well as spectral parameters (see section 3.2.1).For each city, both modelling techniques were developed, and the better-performing modelwas subsequently applied to the complete spatial grids covering the test cities to generate spatially continuous temperature estimates for heatwave conditions to analyse heat exposure.

The results were validated using the statistical error measuresMean Absolute Error (MAE) and Root Mean Squared Error (RMSE), based on a 10-fold cross-validation procedure in which the dataset was repeatedly split into training and test subsets and the performance metrics were averaged across all sections.Both metrics are widely used to measure model performance (Chai & Draxler, 2014), and provide information about the average model-prediction error, in this study expressed in degree Celsius. Compared to MAE, RMSE gives more weight to outliers (Willmott & Matsuura, 2005). Moreover, two heat-specific validation metrics were applied to assess the model's performance under extreme heat conditions. Heat-days are defined as days with maximum air temperatures of at least 30°C (EEA, 2021). This is particularly important because a model may show low overall MAE or RMSE while still misrepresenting extreme temperatures during heatwave situations. The first metric is theProbability of Detection (POD) adjusted to heat-days, defined as the fraction of observed heat-daysthat were correctly classified by the model. POD ranges from 0 to 1, with values close to 1 indicating a high ability to detect heat events (NOAA a, 2026, Mohapatra et al., 2025, Developmental Testbed Center, 2009). In the context of this study (modelling heatwave extreme scenarios), POD therefore evaluates the spatial consistency between observed and modelled heat-day locations. High values indicate that the model correctly identified those locations that experienced extreme heat during the observed heatwave.In addition, the Mean Error onhot days (also referred to as hot-day Bias) is used as a fourth evaluation metric. It quantifies the difference between the mean of predicted heat-day temperaturesand the mean of observedheat-day temperatures (maximum temperature ≥ 30°C), giving information about over- or underestimation of extreme heat.Values close to zero indicate a minimal bias(Stanski et al., 1989, NOAA a, 2026, NOAA b, 2026).Together, these two heat-specific metrics allow the assessment of model performance under extreme heat conditions. POD assesses the spatial agreement in the identification of heat-affected areas, while the hot-day bias evaluates the accuracy of the modelled heat intensity within these areas.

3.3.2 Development of theHeat Vulnerability Index

Building on existing studies that link population vulnerability to thermal exposure, a HVI was developed to integrate both heat exposure and population susceptibility at the grid-cell level (e.g.Rupp et al., 2026, Zhang et al., 2019, Johnson et al, 2012). Heat exposure is represented by spatially modelled daily maximum air temperatures during heatwave conditions, while population vulnerability is approximated using age-specific population groups, following established findings in the literature.Based on evidence indicating increased heat-related health risks, population groups aged 65+ years were classified as highly vulnerable, whilechildren below 3 years of age as vulnerable (e.g. United Nations Children's Fund, 2023, Arsad et al., 2022,Azan et al., 2015,Hajat et al., 2007). Children under three years were considered slightly less vulnerable (weighting factor 0.3) than the 65+ age group (weighting factor 0.4), as epidemiological studies show that heat-related mortalityis higher among older adults (e.g. An der Heiden et al., 2020, Linares & Díaz, 2008).All remaining age groups were considered to exhibit comparatively low heat-related vulnerability (weighting factor 0.1).

Prior to index construction, all input variables were z-standardised, resulting in a mean of zero and a standard deviation of one for each indicator. This standardisation ensures comparability among variables measured on different scales and enables their weighted combination(e.g. Ko et al., 2021, Guo et al., 2019).

The social component of the index was calculated as a weighted linear combination of the standardised age-group indicators, representing social heat vulnerability (0.4 for age groups above 65 and 0.3 for age groups below three). To account for heat exposure, this social vulnerability component was subsequently multiplied by the standardisedmodelled maximum air temperature per grid cell. The resulting exposure-weighted HVI thus highlights locations where high population vulnerability coincides with elevated heat exposure.Finally, the continuous HVI values were classified into three relative vulnerability classes (Low, Medium, High) using the 33rd and 66th percentiles as class thresholds. This quantile-based classification facilitates a relative comparison of heat vulnerability patterns within each test city.

4 RESULTS

This section explains the results of the heatwave modellingapproaches and the results of the calculation of the HVI for all three test cities.

4.1 Heatwave Models

The results of the heatwave models, portraying the spatial distribution of maximum air temperatures observed during a real heatwave period, are shownin Fig. 3, with the corresponding statistical metrics summarisedin Table 2. For Augsburg, PLS performed best with an RMSE of 2.73°C, a MAE of 2.23°C, a hot-day Bias of -2.59°C, and a POD of 1. The relatively high RMSE indicates that the model occasionally produces larger errors, particularly on the hottest days, as this metric gives more weight to outliers (here, maximum temperatures). The MAE is slightly lower, as it is less sensitive to extreme values, reflecting that the model performs well on average. Nevertheless, the mean error remains around 2°C. The hot-day Bias reveals a systematic underestimation of heat intensity at the loggers' locations. Despite this, all heat-day locations (POD = 1) were correctly captured, demonstrating strong spatial agreement during the heatwave scenario. In Hamm, PLS was also used to model the areawide heatwave situation. With an RMSE of 2.89°C, Hamm exhibits the highest overall deviations among the three test cities, indicating the presence of potentialtemperature outliers. The MAE of 2.32°C indicates generally accurate predictions despite these deviations. Thehot-day Bias is the smallest among the three test cities at -0.24°C, reflecting only a minor underestimation of extreme heat intensities. Similar to Augsburg, all heat-day locationswerecaptured correctly (POD = 1), indicating excellent spatial detection at the sensor locations. In Zwickau, RF outperformed PLS, particularly in visual comparison (not shown). The heatwave model achieves the best statistical validation metrics, with anRMSE of 1.57°C and a MAE of 0.96°C, indicating very low deviations and high accuracy. The hot-day Bias shows a small underestimation (-0.59°C), while POD = 1 confirms that all heat-day locations were correctly identified at the logger sites.

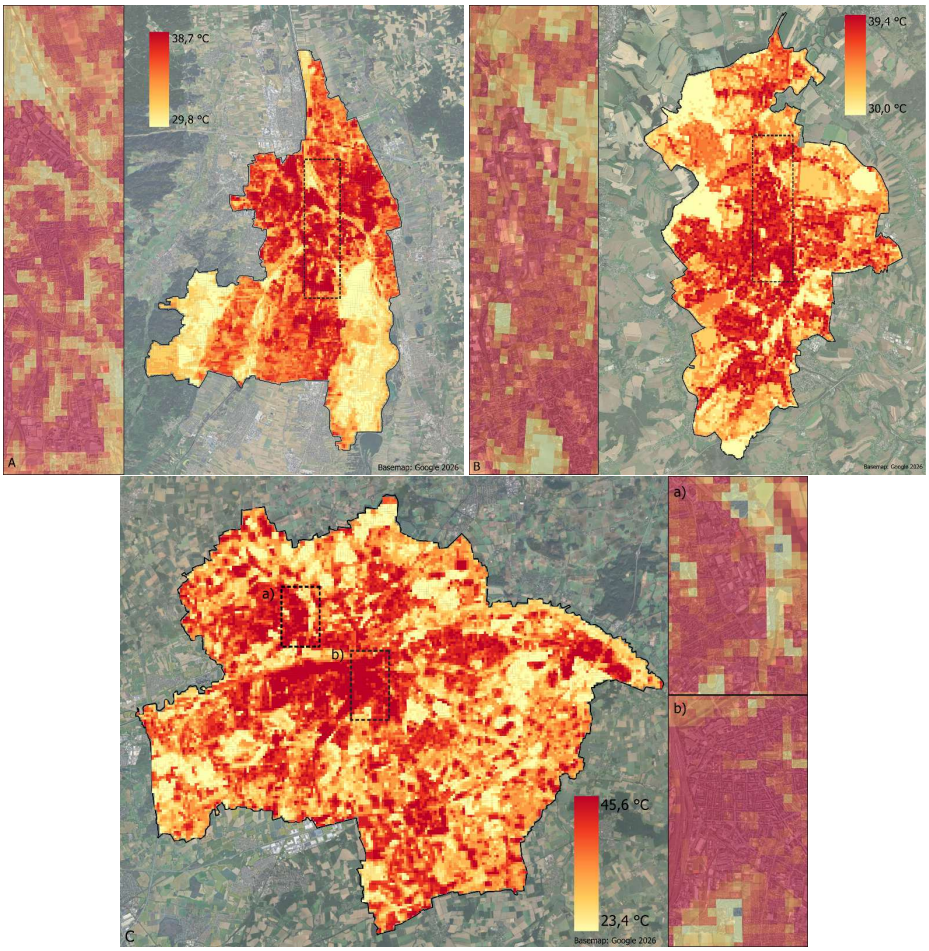

Figure 3: Heatwave model results for Augsburg (A), Zwickau (B), and Hamm (C).

In the cartographic representation (Fig.3), the hottest locations are generally located in the inner-city districts and industrial areas (dark red), whereas forested zones remain comparatively cool (light yellow). In Augsburg (A) the zoomed-in area shows the inner city of Augsburg, along with the surrounding northern and southern districts. Maximum temperatures reach nearly 39 °C in the city centre and industrial zones, while areas along the rivers and water structures as well as more forested areas, remain the coolest. In Zwickau (B), the close-up view shows the inner city in the south extending northward into industrial areas, with temperatures reaching nearly 40 °C. Cooler areas are observed around the inner-city water body and a park. For Hamm (C), two zoomed-in areas are presented: Zoom a) highlights an industrial area with high temperatures, surrounded by cooler forested zones, while Zoom b) shows the city centre with maximum temperatures reaching up to 45°C.

	Model	RMSE[°C]	MAE[°C]	Hot-day Bias [°C]	POD
Augsburg	PLS	2.73	2.23	-2.59	1
Zwickau	RF	1.57	0.96	-0.59	1
Hamm	PLS	2.89	2.32	-0.24	1

Table 2: Validation metrics results for the three test cities Augsburg, Zwickau, and Hamm.

4.1.1 Heat Vulnerability Index

The results ofthe exposure weighted HVI are presented in in Fig.4, with the heatwave models shown beneath with transparency. The HVI is only displayed for areas where the census data provide population information. Therefore, non-built-up areas and industrial zonesare excluded (dark red areas in the background, where heat intensity is also high during heatwaves).

For all three cities, locations within the inner-city districts (zoomed excerpts) exhibit predominantly high HVI values, indicating that these areas experience both elevated heat exposure and a comparatively large population of residents above 65 years of age or below 3 years of age. However, cells with a high HVI are not confined to the inner-city districts. As Fig. 4 illustrates, high HVI values are distributed across the urban areas, highlighting locations where extreme heat exposure coincides with a high age-related social vulnerability regarding heat related health risks. Medium and low HVI zones are predominantly scattered throughout suburban and less densely built-up areas, even though also present in the inner-city areas.

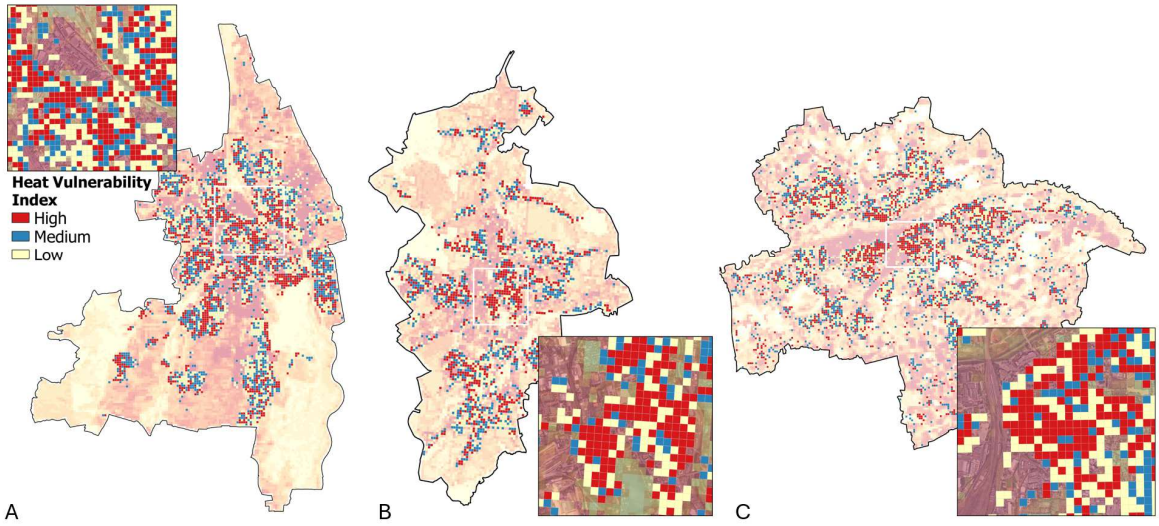

Figure 4: Heat Vulnerability Index for Augsburg (A), Zwickau (B), and Hamm (C).

5 DISCUSSION

In general, this study demonstrates that the proposed approach –combining multisensor remote sensing data, machine learning techniques, CS air temperature measurements, and census data–enables the robust identification of urban heat hotspots. Importantly, the analysis goes beyond the assessment of heat exposure alone by explicitly incorporating social vulnerability, thereby capturing not only where the hottest locations are, but also where vulnerable populations are most affected.

This integrated perspective is particularly valuable for the development of targeted heat adaptation strategies, as it highlights neighbourhoods where elevated heat exposure coincides with a high proportion of vulnerable age groups. The identification of these hotspots provides a critical basis for urban planning, public health

interventions, and resource allocation, supporting more effective mitigation ofheat-related health impacts during heatwave events.

Despite the overall validity and usefulness of the results, several methodological limitations, uncertainties within the CS data (e.g. bias due to logger design or missing validation with an official networkas part of this study) and potential improvementsshould be acknowledged. Concerning the heatwave temperature models, the results indicate that a systematically transferable temperature model across cities is not yet achievable. Instead, city-specific adaptation of temperature data is required, particularly when the available data volume is limited.As demonstrated in the case of Hamm and Zwickau, in comparison with Augsburg, where there are many more data loggers available, insufficient data coverage may not adequately compensate for local biases. Furthermore, if the data pool does not sufficiently represent all LCZ, e.g. only one sensor representing industrial areas in Hamm or only one sensor representing open green space and near water areas in Zwickau, model performance can be reduced, and therefore, the input CS temperature data had to be adapted manually beforehand. In addition, the statistical metrics did not always indicate optimal model performance. However, this limitation is of secondary importance for the primary objective of this study, which focuses on identifying the relative spatial distribution of the most heat-exposed areas, rather than exact temperature values. Systematic over- or underestimation of absolute temperature does not substantially affect the identification of relative heat hotspots within the urban context. Moreover, model experiments during the modelling process revealed that very good statistical performance can sometimes coincide with visually unrealistic spatial patterns, e.g. predicting industrial or densely built-up areas as cooler than adjacent largervegetated areas, highlighting the importance of combining quantitative validation with qualitative, visual evaluation within the framework of using CS data.

It is also important to acknowledge that air temperature measurements obtained through CS approaches represent a valuable data source; however, they capture only near-surface air temperature and not the heat stress actually experienced by people, which results from a combination of air temperature, humidity, radiation, and wind (Oke et al., 2017).

Beyond these methodological aspects, the assessment of social vulnerability could be further refined in future research. In the present study, vulnerability related to age structure was considered based on existing studies and the thresholds used; however, evidence from studies suggests that heat-related health risks increase substantially with advancing age (e.g. Arsad et al., 2022, Benmarhnia et al., 2015). Differentiating weighting factors within the elderly population, for example,higher vulnerability for age groups above 75 years, could therefore potentially improve the representation of heat susceptibility. In addition, further vulnerability indicators such as income level or housing conditions could be incorporated to better reflect adaptive capacity, which was not explicitly accounted for in this analysis (e.g. Rupp et al., 2026,Kohon et al., 2024). Including such socioeconomic variables would allow for a more comprehensive characterisation of population vulnerability and resilience to extreme heat events. Wilson et al. (2024) recently demonstrated that heat related health risks seem to be strongly dependent on external circumstances.

Moreover, the current vulnerability assessment is temporally static and does not account for variations in population exposure over the course of the day or between weekdays and weekends. However, people's spatial distribution and activity patterns differ between daytime and nighttime, as well as between working days and weekends. A time-dependent analysis could therefore provide more realistic insights into heat exposure and associated risks, particularly by capturing commuting patterns and daily mobility. Related to this, industrial and commercial areas were excluded from the vulnerability analysis due to the absence of census data. Nevertheless, these areas can host large numbers of workers during daytime hours on weekdays and may thus represent significant, yet currently unaccounted-for, zones of heat exposure. Incorporating daytime population data or workplace-related exposure estimates would further enhance the realism and applicability of the vulnerability assessment, especially for occupational heat risk management.

6 CONCLUSION

Overall, this study provides a robust and transferable methodological framework for the identification of urban heat risk by integrating temperature exposure during heatwave conditions with social vulnerability indicators. Despite existing limitations, the results offer valuable insights for heat risk management and demonstrate the added value of combining environmental exposure with demographic vulnerability. The

proposed approach therefore represents a meaningful contribution to urban climate research and offers a solid foundation for future refinements and practical applications in heat adaptation planning.

7 ACKNOWLEDGEMENTS

This research was funded by the Federal Ministry for the Environment, Nature Conservation, Nuclear Safety and Consumer Protection as part of the funding programme for measures to adapt to the impacts of climate change (DAS), grant number 67DAS255, HEATS – Urban heat risk management. Project period: 01/06/2023 – 30/11/2025.

Additionally, we kindly thank all owners of Citizen Weather Stations, CWS, who shared their data and this way, made the analysis possible, as well as Jonas Kittner and collegues from Ruhr-Universität Bochum for providing the data within the HEATS framework.

8 REFERENCES

Amt für Statistik und Stadtforschung der Stadt Augsburg: Statistik Augsburg interaktiv. 2026. URL: Statistik Augsburg interaktiv . (Accessed 17.01.2026).

An der Heiden, M., Muthers, S., Niemann, H., Buchholz, U., Grabenhenrich, L. & Matzarakis, A.: Heat-Related Mortality: An Analysis of the Impact of Heatwaves in Germany Between 1992 and 2017. In: Deutsches Ärzteblatt International, Vol. 116, Issue 31-32, pp. 521-528. 2020.

Aram, F., Higueras García, E., Solgi, E. & Mansournia, S.: Urban green space cooling effect in cities. In: Heliyon, Vol. 5, Issue e01339. 2019.

Arsad, F.S., Hod, R., Ahmad, N., Ismail, R., Mohamed, N., Baharom, M., Osman, Y., Radi, M.F.M. & Tangang, F.: The Impact of Heatwaves on Mortality and Morbidity and the Associated Vulnerability Factors: A Systematic Review. In: Int. J. Environ. Res. Public Health, Vol. 19, Issue 16356. 2022.

Aslan, N. & Koc-San, D.: Analysis of Relationship between Urban Heat Island Effect and Land Use/Cover Type using Landsat 7 ETM+ and Landsat 8 OLI Images. In: The International Archieves of the Phogrammetry, Remote Sensing and Spatial Information Sciences, Vol. XLI-B8, XXIII ISPRS Congress. Prague, 2016.

Azan, A., Nyimbili, S., Babayode, O.O., Bershteyn, A.: Exceeding the limits of paediatric heat stress tolerance: the risk of losing a generation to climate inaction. In: BMJ Peadiatrics Open, Vol. 9, Issue e002883. 2025.

Bechtel, B., Kittner, J., Fenner, D., and Demuzere, M.: A Global Database of quality-controlled Crowd Weather Station Data. EGU General Assembly 2024. EGU24-1788, Vienna, 2024.

Beck, H.E., Zimmermann, N.E., McVicar, T.R., Vergopolan, N., Berg, A. & Wood, E.F.: Data Descriptor: Present and future Köppen-Geiger climate classification maps at 1-km resolution. In: Scientific Data, Vol. 5, Issue 180214. 2018.

Benmarhnia, T., Deguen, S., Kaufman, J.S. & Smargiassi, A.: Vulnerability to Heat-related Mortality: A Systematic Review, Meta-analysis, and Meta-regression Analysis. In: Epidemiology, Vol. 26, Issue 6, pp.781-793. 2015.

Breimann, L.: Random Forests. In: Machine Learning, Vol. 45, Issue 1, pp. 5-32. 2001.

Chai, T. & Draxler, R.R.: Root mean square error (RMSE) or mean absolute error (MAE)? – Arguments against avoiding RMSE in the literature. In: Geosci. Model Dev., Vol. 7, pp. 1247-1250. 2014.

gilabertChen, Q., Ding, M., Yang, X., Hu, K. & Qi, J.: Spatially explicit assessment of heat health risk by using multi-sensor remote sensing images and socioeconomic data in Yangtze River Delta, China. In: Int. J. Health Geogr., Vol. 17, Issue 15. 2018.

Climate-Data.org a: Klima Augsburg.2026. URL:Klima Augsburg: Wetter Augsburg und Temperatur nach Monaten für Augsburg . (Accessed 17.01.2026).

Climate-Data.org b: Klima Hamm. 2026. URL: Klima Hamm: Wetter Hamm und Temperatur nach Monaten für Hamm . (Accessed 17.01.2026).

Climate-Data.org c: Klima Zwickau. 2026. URL:Klima Zwickau: Wetter Zwickau und Temperatur nach Monaten für Zwickau . (Accessed 17.01.2026).

Developmental Testbed Center (DTC): Model Evaluation Tools Version 2.0 (METv2.0). User's Guide. Boulder, 2009.

Dodman, D., Hayward, B., Pelling, M., Castan Broto, V., Chow, W., Chu, E., Dawson, R., Khirfan, L., McPhearson, T., Prakash, A., Zheng, Y. & Ziervogel, G.: Cities, Settlements and Key Infrastructure. In: Climate Change 2022: Impacts, Adaption and Vulnerability. Contribution of Working Group II to the Sixth Assessment Report of the Intergovernmental Panel on Climate Change [Pörtner, H.-O., Roberts, D.C., Tignor, M., Poloczanska, E.S., Mintenbeck, K., Alegria, A., Craig, M., Langsdorf, S., Löschke, S., Möller, V., Okem, A. & Rama, B. (eds.)]. Cambridge, UK and New York, USA, 2022.

Dong, J., Peng, J., He, X., Corcoran, J., Qiu, S. & Wang, X.: Heatwave-induced human health risk assessment in megacities based on heat stress-social vulnerability-human exposure framework. In: Landscape and Urban Planning, Vol. 203, Issue 103907. 2020.

EEA European Environmental Agency: Heat and cold – extreme heat. 2021. URL: Heat and cold — extreme heat | Heat and cold | European Environment Agency (EEA)(Accessed 17.01.2026).

European Comission: INSPIRE Data Specification on Geographical Grid Systems – Technical Guidelines. 2013. URL: https://knowledge-base.inspire.ec.europa.eu/publications/inspire-data-specification-geographical-grid-systems-technical-guidelines_en (Accessed 02.03.2026).

Fenner, D., Bechtel, B., Demuzere, M., Kittner, J., & Meier, F.: CrowdQC+—A QualityControl for Crowdsourced Air-Temperature Observations Enabling World-Wide Urban Climate Applications. In: Frontiers in Environmental Science, Vol. 9, Issue 720747. 2021.

Fenner, D., Grassmann, T., Bechtel, B., Demuzere, M., Kittner, J., & Meier, F.: CrowdQCplus: Enhanced quality control for crowdsourced data from citizen weather stations. 2023.

Friesen, J. & Taubenböck, H.: The world's largest cities under climate change and their adaptive capacity to rising heat. In: Scientific Reports, Vol. 15, Issue 1, Article 32671, 2025.

Geiß, C., Zhu, Y., Qiu, C., Mou, L., Zhu, X.X. & Taubenböck, H.: Deep Relearning in the Geospatial Domain for Semantic Remote Sensing Image Segmentation. In: IEEE Geoscience and Remote Sensing Letters, Vol. 19, Issue 8002705. 2022.

Gilabert, J., Deluca, A., Lauwaet, D., Ballester, J., Corbera, J. & Llasat, M.C.: Assessing heat exposure to extreme temperatures in urban areas using the Local Climate Zone classification. In: Nat. Hazards Earth Syst. Sci., Vol. 21, pp. 375-391. 2021.

Guo, X., Huang, G., Jia, P. & Wu, J.: Estimating fine-scale heat vulnerability in Beijing through two approaches: Spatial patterns, similarities, and divergence. In: Remote Sensing, Vol. 11, Issue 2358. 2019.

Hajat, S., Kovats, R.S. & Lachowycz, K.: Heat-related and cold-related deaths in England and Wales: who is at risk? In: Occup Environ Med, Vol. 64, pp. 93-100. 2007.

Harlan, S.L., Declet-Barreto, J.H., Stefanov, W.L. & Petitti, D.B.: Neighborhood Effects on Heat Deaths: Social and Environmental Predictors of Vulnerability in Maricopa County, Arizona. In: Environmental Health Perspectives, Vol. 121, Issue 2. 2013.

He, R., Wang, J. & Liu, D.: Assessing the Impact of Urban Spatial Form on Land Surface Temperature Using Random Forest – Taking Beijing as a Case Study. In: Land, Vol. 14, Issue 1639. 2025.

IPCC: Climate Change 2022: Impacts, Adaptation and Vulnerability. Contribution of Working Group II to the Sixth Assessment Report of the Intergovernmental Panel on Climate Change. [H.-O. Pörtner, D.C. Roberts, M. Tignor, E.S. Poloczanska, K. Mintenbeck, A. Alegría, M. Craig, S. Langsdorf, S. Löschke, V. Möller, A. Okem, B. Rama (eds.)]. Cambridge University Press. Cambridge University Press, Cambridge, UK and New York, NY, USA, 3056 pp., doi:10.1017/9781009325844. 2022.

Johnson, D.P., Stanforth, A., Lulla, V. & Luber, G.: Developing an applied extreme heat vulnerability index utilizing socioeconomic and eniornmental data. In: Applied Geography, Vol. 32, pp. 23-31. 2012.

Ko, J., Park, U., Kim, D. & Kang, S.W.: Quantitative Electroencephalogram Standardization: A Sex and Age-Differentiated Normative Database. In: Front. Neurosci., Vol. 15, Issue 766781. 2021.

Kohon, J.N., Tanaka, K., Himes, D., Toda, E., Carder, P.C., Carlson, B.: Extreme Heat Vulnerability Among Older Adults: A Multilevel Risk Indes for Portland, Oregon. In: The Gerontologist, Vol. 64, pp.1-10. 2024.

Li, Z.-L., Tang, B.-H., Wu, H., Ren, H., Yan, G., Wan, Z., Trigo, I.F. & Sobrino, J.A.: Satellite-derived land surface temperature: Current status and perpectives. In: Remote Sensing of Environment, Vol. 131, pp.14-37. 2013.

Liu, C., Lu, S., Tian, J., Yin, L., Wang, L. & Zheng, W.: Research Overview on Urban Heat Islands Driven by Computational Intelligence. In: Land, Vol. 13, Issue 2176. 2024.

Linares, C. & Díaz, J.: Impact of heat waves on daily mortality in distinct age groups. In: Gac. Sanit., Vol. 22, Issue 2, pp. 115-9. 2008.

Leichtle, T., Kühnl, M., Droin, A., Beck, C., Hiete, M. & Taubenböck, H. (a): Quantifying urban heat exposure at fine scale – modeling outdoor and indoor temperatures using citizen science and VHR remote sensing. In: Urban Climate, Vol. 49, Issue 101522. 2023.

Leichtle, T., Helgert, S., Müller, M., Handschuh, J., Erbertseder, T. & Wurm, M. (b): Opposing land surface and air temperatures from remote sensing and Citizen Science for quantification of the Urban Heat Island effect. In: 2023 Joint Urban Remote Sensing Event (JURSE), pp. 1-5. Heraklion, 2023.

Meier, F., Fenner, D., Grassmann, T., Otto, M. & Scherer, D.: Crowdsourcing air temperature from citizen weather stations for urban climate research. In: Urban Climate, Vol. 19, pp. 170-191. 2017.

Montensinos López, O.A., Montesinos López, A. & Crossa, J.: Convolutional Neural Networks. Multivariate Statistical Machine Learning Methods for Genomic Prediction. Springer, Cham, 2022.

Mohapatra, M., Srivastava, A., Nadimpalli, R. & Kumar, N.: Evolution of heat wave monitoring and forecasting in India. In: Mausam, Vol. 76, Issue 1, pp.303-316. 2025.

NOAA a: Forecast Verification Glossary. National Oceanic and Atmospheric Administration. 2026. URL: Forecast Verification Glossary.pdf (Accessed 16.01.2026).

NOAA b: Previous Summer Heat Index Forecast Verification. Important Note. 2026. URL: PREVIOUS SUMMER HEAT INDEX FORECAST VERIFICATION (Accessed 17.01.2026).

Oke, T.R., Mills, G., Christen, A. & Voogt, J.A.: Urban Climates. Cambridge University Press. 2017.

Oukawa, G. Y., Krecl, P. & Targino, A.C.: Fine-scale modeling of the urban heat island: A comparison of multiple linear regression and random forest approaches. In: Science of The Total Environment, Vol. 815, Issue 152836. 2022.

PIKOBYTES GmbH: Sensoto – Sensor data at your fingertips. 2026. URL:https://sensoto.io/de/. (Accessed 17.01.2026).

Pirouz, D.M.: An Overview of Partial Least Squares. In: SSRN Electronic Journal. 2006.

Ramachandra, T.V., Rana, R.S., Vinay, S. & Aithal, B.H.: Urban heat island linkages with landscape morphology. In: Scientific Reports, Vol. 15, Issue 24485. 2025.

Reid, C.E., Mann, J.K., Alfasso, R., English, P.B., King, G.C., Lincoln, R.A., Margolis, H.G., Rubado, D.J., Sabato, J.E., West, N.L., Woods, B., Navarro, K.M. & Balmes, J.R.: Evaluation of a Heat Vulnerability Index on Abnormally Hot Days: An Environmental Public Health Tracking Study. In: Environmental Health Perspectives, Vol. 120, Issue 5. 2012.

Rupp, S., Leichtle, T., Beck, C. & Hiete, M.: Where heat adaption is needed most – An open-source approach to developing a transferable heat risk index for urban planning. In: Urban Climate, Vol. 65, Issue 102769. 2026.

Stadt Augsburg (a): Augsburg in Kürze. 2026. URL: Augsburg in Kürze . (Accessed 17.01.2026).

Stadt Ausgburg (b): Hitze-Portal der Stadt Augsburg. 2026. URL: Hitze-Portal . (Accessed 17.01.2026).

Stadt Hamm (a): Gesellschaft, Soziales, Gesundheit. 2026. URL:Überblick | Stadt Hamm . (Accessed 17.01.2026).

Stadt Hamm (b): Klima und Mobilität. 2026. URL: Überblick | Stadt Hamm . (Accessed 17.01.2026).

Stadt Zwickau (a): Bevölkerung. 2026. URL:Bevölkerung - Stadt Zwickau . (Accessed 17.01.2026).

Stadt Zwickau (b): Zahlen, Daten, Fakten. 2026. URL: Zahlen, Daten, Fakten - Stadt Zwickau . (Accessed 17.01.2026).

Stadt Zwickau (c): Stadtklimauntersuchung (Klimafunktionskarte und Planungshinweiskarte).2026. URL:Stadtklimauntersuchung - Stadt Zwickau . (Accessed 17.01.2026).

Stanski, H., Wilson, L.J., Burrows, W.R.: Survey of common verification methods in meteorlogy. Atmospheric Environment Service, Vol. 89-5. Downsview, 1989.

Statistisches Bundesamt (a): Zensus 2022. Bevölkerung. Alter in 5 Klassen. Wiesbaden, 2022. URL:Zensus 2022 - Statistisches Bundesamt. (Accessed 17.01.2026).

Statistisches Bundesamt (b): Zensus 2022. Bevölkerung. Alter in 10er-Jahresgruppen. Wiesbaden, 2022. URL: Zensus 2022 - Statistisches Bundesamt .(Accessed 17.01.2026).

Statistisches Bundesamt (c): Code: 12411-0018. Bevölkerung: Kreise, Stichtag, Geschlecht, Altersgruppen. Wiesbaden, 2026. URL: Bevölkerung: Kreise, Stichtag, Geschlecht, Altersgruppen. (Accessed 17.01.2026).

Statistisches Bundesamt (d): Hamm, Stadt. 2026. URL:05915000 | Statistikportal.de . (Accessed 17.01.2026).

Stewart, I.D. & Oke, T.R.: Local Climate Zones for Urban Temperature Studies. In: Bulletin of the American Meteoorological Society, Vol. 93, Issue 12, pp. 1879-1900. 2012.

Taubenböck, H., Mast, J., Geiß, C., Wurm, M., Esch, T.& Seto, K.: Global differences in urbanization dynamics from 1985 to 2015 and outlook considering IPCC climate scenarios. In: Cities, Vol. 151, Issue 105117. 2024.

United Nations Children's Fund: Protecting Children from Heat Stress. A technical note. New York, 2023.

Voogt, J.A. & Oke, T.R.: Thermal remote sensing of urban climates. In: Remote Sensing of Environment, Vol. 86, pp. 370-384. 2003.

Weng, Q.: Thermal infrared remote sensing for urban climate and environmental studies: Methods, applications, and trends. In: ISPRS Journal of Photogrammetry and Remote Sensing, Vol. 64, pp. 335-344. 2009.

Weigand, M.,Wurm, M., Droin, A.,Stark, T., Staab, J.,Rauh, J.&Taubenböck, H.: Are public green spaces distributed fairly? A nationwide analysis based on remote sensing, OpenStreetMap and census data. In: Geocarto International, Vol. 38, Issue 1, 2286305. 2023.

Willmott, C.J. & Matsuura, K.: Advantages of the mean absolute error (MAE) over the root mean square error (RMSE) in assessing average model performance. In: Climate Research, Vol. 30, pp. 79-82. 2005.

Wilson, A.J., Bressler, R.D., Ivanovich, C., Tuholske, C., Raymond, C., Horton, R.M., Sobel, A., Kinney, P., Cavazos, T. & Shrader, J.G.: Heat disproportionately kills young people: Evidence from wet-bulb temperature in Mexico. In: Science Advances, Vol. 10, Issue 49. 2024.

Zargari, M., Mofidi, A., Entezari, A. & Baaghideh, M.: Climate comparison of surface urban heat island using satellite remote sensing in Tehran and suburbs. In: Scientific Reports, Vol. 14, Issue 643. 2024.

Zhang, W., Zheng, C. & Chen, F.: Mapping heat-related health risks of elderly citizens in mountainous area: A case study of Chongqing, China. In: Science of the Total Environment, Vol. 663, pp. 852-866. 2019.

Zumwald, M., Knüsel, B., Bresch, D.N. & Knutti, R.: Mapping urban temperature using crowd-sensing data and machine learning. In: Urban Climate, Vol. 35, Issue 100739. 2021.